

Equilibrium circulation and stress distribution in viscoelastic creeping flow

Joseph. A. Biello^a, Becca Thomases^{a,*}

^a*Department of Mathematics, University of California, Davis, CA 95616*

Abstract

An analytic, asymptotic approximation of the nonlinear steady-state equations for viscoelastic creeping flow, modeled by the Oldroyd-B equations with polymer stress diffusion, is derived. Near the extensional stagnation point the flow stretches and aligns polymers along the outgoing streamlines of the stagnation point resulting in a stress-island, or birefringent strand. The polymer stress diffusion coefficient is used, both as an asymptotic parameter and a regularization parameter. The structure of the singular part of the polymer stress tensor is a Gaussian aligned with the incoming streamline of the stagnation point; a smoothed δ -distribution whose width is proportional to the square-root of the diffusion coefficient. The amplitude of the stress island scales with the Wiessenberg number, and although singular in the limit of vanishing diffusion, it is integrable in the cross stream direction due to its vanishing width; this yields a convergent secondary flow. The leading order velocity response to this stress island is constructed and shown to be *independent* of the diffusion coefficient in the limit. The secondary circulation counteracts the forced flow and has a vorticity jump at the location of the stress islands, essentially expelling the background vorticity from the location of the birefringent strands. The analytic solutions are shown to be in excellent quantitative agreement with full numerical simulations, and therefore, the analytic solutions elucidate the salient mechanisms of the flow response to viscoelasticity and the mechanism for instability.

Keywords: viscoelastic creeping flow; extensional flow; asymptotic analysis; stress diffusion

1. Introduction

Viscoelastic flows are found in many important engineering and biological systems. Despite the need to understand these flows in a variety of complex situations, analysis of the equations of motion describing viscoelastic fluids,

*Corresponding author

Email addresses: biello@math.ucdavis.edu (Joseph. A. Biello),
thomases@math.ucdavis.edu (Becca Thomases)

even in the low-Reynolds number regime, is very incomplete. There are many different models depending on the rheology of the fluid, but little is known even for the simplest closed continuum models. One popular model, the Oldroyd-B model, can be derived from microscopic principles and represents “Boger” fluids, dilute solutions of polymers immersed in a Newtonian solvent which exhibit normal stress differences but not shear thinning. This model is used frequently in simulations of viscoelastic fluids even though there is no mathematical well-posedness theory for this system, i.e. it is not known if sufficiently smooth solutions to this system exist for all time, bringing in to question the reliability of any numerical simulation.

Flows at internal stagnation points (such as the four-roll mill flow or the cross-slot or cross channel flow) pose a particular difficulty for both theoretical investigation and numerical simulations of viscoelastic fluids, as polymers are aligned and stretched, and can create fine features in the flow that are difficult to resolve numerically. However it is precisely at these points in the flow that interesting dynamics arise. Instabilities have been found in experiments at internal stagnation points [1, 2, 3, 4, 5], and related numerical instabilities are found in similar geometries [6, 7, 8, 9, 10, 11]. It is unclear what is driving these instabilities, but it is reasonable to conjecture that they are related to the large polymer stresses and stress gradients which accumulate along the incoming and outgoing streamlines of these internal stagnation points.

The elastic contribution to the total stress can be incorporated into the equations of motion by assuming that the total stress on the fluid, $\sigma = \tau_s + \tau_p$, comes from a solvent contribution τ_s as well as a polymer contribution τ_p . In the case of a Newtonian solvent, the total stress is given by

$$\sigma = -p\mathbf{I} + \eta_s \dot{\boldsymbol{\gamma}} + \tau_p,$$

where η_s is the Newtonian solvent viscosity, and $\dot{\boldsymbol{\gamma}} = [\nabla \mathbf{u} + \nabla \mathbf{u}^T]$ is the rate-of-strain tensor. Assuming conservation of mass and incompressibility the fluid velocity \mathbf{u} satisfies

$$\rho \frac{D\mathbf{u}}{Dt} = \nabla \cdot \sigma + \mathbf{f}, \quad \nabla \cdot \mathbf{u} = 0,$$

for density ρ , and body force \mathbf{f} , or in the inertialess regime,

$$\nabla \cdot \sigma + \mathbf{f} = 0, \quad \nabla \cdot \mathbf{u} = 0. \tag{1}$$

In the Oldroyd-B model, the symmetric polymer stress tensor, τ_p , is advected via the upper-convected derivative and relaxes with a characteristic relaxation time λ :

$$\tau_p + \lambda \overset{\nabla}{\boldsymbol{\tau}}_p = \eta_p \dot{\boldsymbol{\gamma}}. \tag{2}$$

Here η_p is the polymer viscosity, and the upper-convected derivative is defined by

$$\overset{\nabla}{\mathbf{A}} \equiv \frac{\partial \mathbf{A}}{\partial t} + \mathbf{u} \cdot \nabla \mathbf{A} - (\nabla \mathbf{u} \cdot \mathbf{A} + \mathbf{A} \cdot (\nabla \mathbf{u})^T), \quad \text{where } (\nabla \mathbf{u})_{ij} = \frac{\partial u^i}{\partial x_j}.$$

While Boger fluids are used in many experiments of viscoelastic phenomena, it is not immediately clear that the Oldroyd-B model is a good choice for modeling more general complex fluids. We choose to work with this model due to the generic nature of the upper-convected derivative. This represents a tensorial material derivative and hence will be found in continuum models which advect a macroscopic elastic stress tensor. Some other variants to the Oldroyd-B model include the Giesekus [12], Phan-Thien-Tanner (PTT) [13], and FENE-P models [14]. These models arise from different microscale models of the polymers. All of them introduce a nonlinear relaxation of stress which results in shear-thinning behavior. All of the above-mentioned macroscopic models contain the upper-convected derivative, the dominant source of nonlinearity in the equations, which leads to many of the difficulties and interesting phenomena associated with the Oldroyd-B model [15, 16, 8, 9, 17]. Oldroyd-B is the “simplest” of these models making it a good model for our theoretical work.

A simple modification to the Oldroyd-B model, which will yield smooth and bounded stresses [18, 19], is to add polymer stress diffusion. The addition of stress diffusion can be derived from the kinetic theory of dumbbells [15, 20], but the stress diffusion coefficient is proportional to the square of the ratio of the bead diameter (or polymer radius of gyration) to the flow length-scale, which even in the context of micro-fluidics is minute (on the size of 10^{-6} at most) [21]. To be useful as a regularization in numerical simulations, artificially large polymer stress diffusion is typically needed [22, 18]. However it is useful to note that there is an analytical result [19] which proves that *any* amount of polymer stress diffusion will maintain a smooth and bounded polymer stress. In this manuscript we use polymer stress diffusion to derive an asymptotic expansion, in orders of the square-root of the stress diffusion coefficient, for solutions to the Oldroyd-B model (at zero Reynolds number) in a simple extensional flow geometry. This solution provides information about the effect of the large stress islands, or birefringent strands, on the resultant flow field. In particular, we are able to take the limit as the diffusion goes to zero and recover information about the effect of these stress islands on the flow. Therefore we can determine the first order effect of the stress island on the velocity in the Stokes-Oldroyd-B system.

An important structure of the momentum equation, which we use to guide us, is that at zero-Reynolds number the velocity is one degree smoother than the stress. This implies that at extensional points in the flow, where the stress accumulates, the exact value of the stress is not needed to determine the effect on the velocity. Only the integral of the stress affects the velocity field. The stress island can be approximated by a smoothed Dirac δ -distribution. Furthermore, when stress diffusion is included in the model, a Gaussian becomes an exact solution of the asymptotic approximation for the stress tensor.

The Gaussian has a well-defined integral even in the limit of zero diffusion which enables us to close the asymptotic expansion and give a well defined solution for the velocity. The result of the transversely narrow and sharply peaked stress distribution is a dip in the velocity whose magnitude is independent of the stress diffusion. Such a dip in the velocity field has been observed experi-

mentally [23, 24] and provides a possible mechanism for the instabilities seen in numerical simulations [6, 7, 8, 9, 10, 11]. Simply stated, the instability mechanism is due to the fact that at extensional points in the flow the vorticity is low. In the low vorticity region, the stress can grow and where the stress is large the vorticity is expelled, leaving a larger area for the stress to begin to oscillate and become unstable. Boundary layer approximations near extensional stagnation points that depend on the polymer extension length and relaxation time were presented in [25, 26].

In what follows we will describe the model and assumptions and derive an asymptotic expansion for the stress and velocity to first order in the stress diffusion coefficient. We conclude by showing that the solutions to our model agree extremely well with numerical simulations. The model captures both the leading order velocity response, as well as the amplitude of the stress in the birefringent strands.

1.1. Model

To perform the analysis it is simpler to write Eqs. (1)-(2) in terms of a conformation tensor, \mathbf{S} , defined by

$$\mathbf{S} = Wi\xi^{-1}\boldsymbol{\tau}_p + \mathbb{I}. \quad (3)$$

The addition of a polymer stress diffusion term, $\nu\Delta\mathbf{S}$ is added to the stress advection equation. This is necessary to our analysis, and we perform the asymptotic expansion in orders of the stress diffusion coefficient ν . In non-dimensional form we write the Stokes-Oldroyd-B equations with polymer diffusion as

$$\Delta\mathbf{u} - \nabla p + \xi Wi^{-1}\nabla \cdot \mathbf{S} + \mathbf{f} = 0, \text{ and } \nabla \cdot \mathbf{u} = 0, \quad (4)$$

$$Wi \overset{\nabla}{\mathbf{S}} + (\mathbf{S} - \mathbb{I}) = \nu\Delta\mathbf{S}. \quad (5)$$

The Weissenberg number, $Wi = \lambda/\tau_f$, is the ratio of the elastic relaxation time to the characteristic flow time-scale, set by \mathbf{f} which we set to unity, and $\xi = \eta_p/\eta_s$ is the ratio of polymer to solvent viscosity.

1.2. Outline of solution strategy

The objective of this work is to find an analytic, asymptotic approximation of Eqs. (1)-(2) at steady state. Our analytical strategy has a few key steps which exploit both the structure of the upper convective derivative and the linearity of the stress feedback on the Stokes equations. Our steps will proceed as follows.

1. We rescale the velocity field by Wi , yielding a factor of Wi which multiplies the pressure and the force, \mathbf{f} . After the rescaling, Wi does not appear in the advection/diffusion equation for the stress.
2. In the rescaled variables, we choose a simple background flow, \mathbf{u} , to drive the dynamics of the upper convective derivative, without specifying the force, \mathbf{f} , which creates this flow. *Crucially* the flow we choose has the

property $\partial_y u = 0$ everywhere. Physically speaking, this is a flow whose vorticity is zero near the maximum of the stress island. In constructing the solution, we will see that the stress feedback on the flow also produces a velocity field whose vorticity vanishes at the maximum of the stress island. Additionally, the feedback flow tends to expel vorticity from the vicinity of the maximum of the stress.

The flow we choose is only intended to describe the local structure of a generic flow near a stress island. This allows us to solve the stress equation because when the stress diffusion coefficient is small the stress equation is essentially hyperbolic, and therefore local in the velocity field.

Mathematically, a flow with this structure causes the equation for the conformation tensor to decouple into a hierarchy of three inhomogeneous, non-constant coefficient linear PDEs. The first component of the conformation tensor, S_{11} , is forced by a constant. The second component, S_{12} , is forced by the solution for S_{11} , and the third component, S_{22} , is forced by S_{12} .

The Oldroyd-B model is most physically relevant in the limit of vanishing stress diffusivity, ν . This motivates an anisotropic scaling of the spatial coordinates typical of boundary layer theories. The resulting linear PDE can then be solved analytically, thereby providing the profile of the conformation tensor.

3. From the form of the Stokes' equation, Eq. (4), the conformation tensor feeds back onto the flow through its divergence, whose components we define as Q_1 and Q_2 as follows:

$$\begin{aligned} Q_1 &\equiv \partial_x S_{11} + \partial_y S_{12} \\ Q_2 &\equiv \partial_x S_{12} + \partial_y S_{22}. \end{aligned} \tag{6}$$

However, since the diffusion is small, and the equations for the components of the tensor break up into a hierarchy of inhomogeneous equations, we show that only Q_1 , the component of the stress divergence in the direction of the axis of localization, is needed to compute the lowest order effect of the stress on the flow.

We use Q_1 to compute the velocity field which arises as a response to the stress. For this problem, we use the classical boundary layer matching techniques whereby the flow is computed in the outer and inner regions separately, and then the two solutions are matched. The inner region corresponds to the layer where the stress divergence, Q_1 , is concentrated.

4. At this point, having prescribed the total velocity (at least locally near the stress island), the conformation tensor and the velocity field induced by the conformation tensor are computed. Since the components of the conformation tensor are sharply localized in stress islands, they are therefore only affected by the velocity field in the vicinity of this localization. By requiring that the total velocity - that due to the forcing plus that due to the stress response - be consistent along the axis of localization of

the stress tensor, we are able to establish a simple linear equation for the saturated amplitude of the conformation tensor.

2. Asymptotic approximation of stress islands and their induced flow

We will first perform all of the calculations in the case of a single stress island in a domain which is infinite in y and periodic in x . The essence of the calculation is captured by this example, which can easily be generalized to doubly periodic domains for purposes of comparison to numerical simulations in the 4-roll mill geometry. We assume periodicity in x for simplicity and consider an extensional flow centered at the origin, with incoming streamlines aligned along the y -axis and outgoing streamlines aligned along the x -axis. In order to create a stress island of finite length along the x -axis, it is necessary that the flow turn around at some $|x| > 0$, and then point away from the x -axis; this will certainly hold in any physical flow. Furthermore, by choosing a functional form which is separable in (x, y) the calculation for obtaining the dependence of the conformation tensor, \mathbf{S} on x , becomes straightforward.

2.1. Rescaling the velocity

In order to simplify the presentation of our calculation it is convenient to rescale the velocity field by Wi . Let $\tilde{\mathbf{u}} = Wi \mathbf{u}$, and $\tilde{p} = Wi p$, then the steady state system of equations becomes

$$\Delta \tilde{\mathbf{u}} - \nabla \tilde{p} + \frac{1}{2} \nabla \cdot \mathbf{S} + Wi \mathbf{f} = 0, \text{ with } \nabla \cdot \tilde{\mathbf{u}} = 0, \quad (7)$$

$$\tilde{\mathbf{u}} \cdot \nabla \mathbf{S} - (\nabla \tilde{\mathbf{u}} \mathbf{S} + \mathbf{S} \nabla \tilde{\mathbf{u}}^T) + (\mathbf{S} - \mathbb{I}) = \nu \Delta \mathbf{S}. \quad (8)$$

We have set the viscosity ratio ξ to $1/2$, for convenience. Since equation (7) is linear we can split the velocity $\tilde{\mathbf{u}} = \mathbf{u}_f + \mathbf{u}_s$ where \mathbf{u}_f solves

$$\Delta \mathbf{u}_f - \nabla p_f + Wi \mathbf{f} = 0 \quad (9)$$

i.e. \mathbf{u}_f is the response of the flow field to the background forcing. and \mathbf{u}_s solves

$$\Delta \mathbf{u}_s - \nabla p_s + \frac{1}{2} \nabla \cdot \mathbf{S} = 0 \quad (10)$$

so \mathbf{u}_s is the stress response. Rather than specify \mathbf{f} , we prescribe the total flow, $\tilde{\mathbf{u}}$, independent of Wi . Clearly from (9), the background flow, \mathbf{u}_f , is linear in Wi , while the induced flow is linear in the amplitude of the conformation tensor.

Equation (8) is linear in \mathbf{S} and, because of the re-scaling of the velocity field, the Weissenberg number does not appear in this equation. Therefore the forced portion of the flow must add to the stress induced portion of the flow to give a total scaled flow ($\tilde{\mathbf{u}}$) which is independent of Wi near the region where \mathbf{S} is localized. This means that the re-scaled flow near the stress island is universal, independent of Weissenberg number. We are free to choose a form of the velocity field, $\tilde{\mathbf{u}}$, in equation (8) which is valid locally near the stress island,

determine the stress profile generated by this velocity field and then determine the flow, \mathbf{u}_s , induced by this velocity field. The induced velocity, \mathbf{u}_s , will be exponentially localized near the stress island and its functional form will coincide with \mathbf{u}_f there. According to equation (9), \mathbf{u}_f is linear in Weissenberg number. Therefore, the requirement that $\tilde{\mathbf{u}}$ is independent of Weissenberg number near the stress island will yield a linear relation for the amplitude of the conformation tensor in terms of the Weissenberg number.

We will write the rescaled total velocity as $\tilde{\mathbf{u}} = u\hat{i} + v\hat{j}$, so that the equation for the upper convected derivative of the stress (8) is written explicitly as

$$[u\partial_x + v\partial_y]\mathbf{S} - \begin{bmatrix} 2(\partial_x u S_{11} + \partial_y u S_{12}) & \partial_x v S_{11} + \partial_y u S_{22} \\ \partial_x v S_{11} + \partial_y u S_{22} & 2(\partial_x v S_{12} + \partial_y v S_{22}) \end{bmatrix} + (\mathbf{S} - \mathbf{I}) = \nu\Delta\mathbf{S}. \quad (11)$$

2.2. The total velocity field

An incompressible 2-D flow can be described in terms of a stream function $\tilde{\mathbf{u}} = u\hat{i} + v\hat{j} = -\partial_y\psi\hat{i} + \partial_x\psi\hat{j}$ with vorticity $\omega = \partial_x v - \partial_y u = \Delta\psi$. Taking the curl of (10), the vorticity induced by the stress satisfies the Poisson equation

$$\Delta\omega_s = \frac{1}{2}(\partial_y Q_1 - \partial_x Q_2) \quad (12)$$

where the induced vorticity, velocity and stream function are related through $\omega_s = \partial_x v_s - \partial_y u_s = \Delta\psi_s$.

Consider the simple stream function

$$\psi = -y \sin(x) \quad (13)$$

whose velocity field is

$$\begin{bmatrix} u \\ v \end{bmatrix} = \begin{bmatrix} \sin(x) \\ -y \cos(x) \end{bmatrix}. \quad (14)$$

The salient properties of the flow (14) are that it has an extensional point at $(x, y) = (0, 0)$, its vorticity is proportional to the stream function

$$\omega = y \sin(x), \quad (15)$$

(which vanishes along the x -axis) and its deformation tensor is

$$\begin{bmatrix} \partial_x u & \partial_y u \\ \partial_x v & \partial_y v \end{bmatrix} = \begin{bmatrix} \cos(x) & 0 \\ y \sin(x) & -\cos(x) \end{bmatrix}. \quad (16)$$

The flow (14) is not an exact solution of the stationary Stoke-Oldroyd-B equations, but it is a useful canonical flow if one considers how a stress island is generated. A circulation like (14) moves fluid toward the origin along the y -axis and away from the origin along the x -axis. As a consequence of this flow, a stress island is formed along the x -axis. Since the stress diffusion, ν , is small, the stress island is confined to a thin layer around the x -axis. Through the

Stokes equations, the stress island generates a secondary circulation which, in the vicinity of the stress island, tends to counteract the original flow. However, since the stress island is strongly confined to the x -axis, it only responds to the primary (\mathbf{u}_f) and secondary (\mathbf{u}_s) circulation in its vicinity. The flow in (14) is simply the first term in the Taylor series in y (near $y = 0$) and a Fourier series in x of any general flow, which is also periodic in x . Therefore, locally about the x -axis, any periodic flow would have a leading order term proportional to (14).

The choice of a periodic function in x is also not arbitrary. If the flow was instead $(u, v) \propto (x, -y)$, it would not recirculate, and the resulting stress island would be infinitely long and invariant along the x -axis.

2.3. Solution of the conformation tensor equations

Substituting the velocity field in (14) to the equations in (11), the equations for the conformation tensor become

$$\begin{aligned} \sin(x) \partial_x S_{11} - y \cos(x) \partial_y S_{11} + [1 - 2 \cos(x)] S_{11} - 1 &= \nu \Delta S_{11} \\ \sin(x) \partial_x S_{12} - y \cos(x) \partial_y S_{12} + S_{12} - y \sin(x) S_{11} &= \nu \Delta S_{12} \\ \sin(x) \partial_x S_{22} - y \cos(x) \partial_y S_{22} + [1 + 2 \cos(x)] S_{22} - 2y \sin(x) S_{12} - 1 &= \nu \Delta S_{22} \end{aligned} \quad (17)$$

These equations have a simple structure, three aspects of which are very illuminating. They each have an inhomogeneity, the S_{11} equation has a constant, 1, the S_{12} equation has $y \sin(x) S_{11}$ and the S_{22} equation has $2y \sin(x) S_{12} - 1$. The first order y -derivatives on the left hand sides are multiplied by y , with no other functional dependence on y . Therefore, there is no additional y scale associated with transport and stretching; however, there is a y scale associated with stress diffusion. The antisymmetry of the inhomogeneities coupled with the symmetry of the linear operator results in S_{11} and S_{22} being symmetric and S_{12} being antisymmetric about the y -axis.

2.3.1. Anisotropic scaling of coordinates

In the limit that $\nu \rightarrow 0$ we can approximately solve the conformation tensor equations (17) by stretching the y -coordinate

$$\frac{y}{\sqrt{\nu}} = Y \implies \frac{\partial}{\partial y} = \frac{1}{\sqrt{\nu}} \frac{\partial}{\partial Y} \quad (18)$$

where we assume that derivatives with respect to Y are $O(1)$. As in boundary layer theories the x -coordinate is not rescaled. This is tantamount to assuming that y -derivatives are $O(\nu^{-\frac{1}{2}})$ larger than x -derivatives.

Performing the rescaling on equations (17) and retaining the lowest order terms in ν removes second derivative terms in x and we find the equation for S_{11} is a linear, inhomogeneous PDE independent of S_{12} and S_{22} ,

$$\sin(x) \partial_x S_{11} - Y \cos(x) \partial_Y S_{11} + [1 - 2 \cos(x)] S_{11} - \partial_Y^2 S_{11} = 1. \quad (19)$$

The equation for S_{12} is also linear, with an inhomogeneity which depends on $\sqrt{\nu}S_{11}$,

$$\sin(x) \partial_x S_{12} - Y \cos(x) \partial_Y S_{12} + S_{12} - \partial_{YY}^2 S_{12} = Y \sin(x) \sqrt{\nu} S_{11}. \quad (20)$$

Finally, the equation for S_{22} is also linear, with an inhomogeneity which depends on $\sqrt{\nu}S_{12}$,

$$\begin{aligned} \sin(x) \partial_x S_{22} - Y \cos(x) \partial_Y S_{22} + [1 + 2 \cos(x)] S_{22} - \partial_{YY}^2 S_{22} \\ = 2Y \sin(x) \sqrt{\nu} S_{12} + 1. \end{aligned} \quad (21)$$

This is typical of boundary layer scaling, and implies that the stress tensor will be elongated along the x -axis.

It is clear that a solution of the system (19) - (21) results in an asymptotic ordering

$$O(S_{12}) \sim \sqrt{\nu} O(S_{11}) \quad \text{and} \quad O(S_{22}) \sim \nu O(S_{11}). \quad (22)$$

However, it is the derivatives of S_{ij} , i.e. Q_1 and Q_2 from Eq. (12), that drive the response of the fluid to the induced stress. Since partial derivatives with respect to y are a factor of $\nu^{-\frac{1}{2}}$ greater than partial derivatives with respect to x , we estimate the order of Q_1 (Eq. 6) by

$$\begin{aligned} O(Q_1) &\sim O(S_{11}) + \nu^{-\frac{1}{2}} O(S_{12}) \\ &\sim O(S_{11}) + \nu^{-\frac{1}{2}} \nu^{\frac{1}{2}} O(S_{11}) \\ &\sim O(S_{11}), \end{aligned} \quad (23)$$

which is to say that both terms which define Q_1 contribute at the same order of magnitude (in ν) to the stress induced velocity field. Similarly for Q_2

$$\begin{aligned} O(Q_2) &\sim O(S_{12}) + \nu^{-\frac{1}{2}} O(S_{22}) \\ &\sim \nu^{\frac{1}{2}} O(S_{11}) + \nu^{-\frac{1}{2}} \nu O(S_{11}) \\ &\sim \nu^{\frac{1}{2}} O(S_{11}), \end{aligned} \quad (24)$$

which is to say that both terms which define Q_2 are of the same order, that being $\sqrt{\nu}$ smaller than Q_1 .

Comparing the terms on the right hand side of (12) we find

$$\begin{aligned} O(\partial_x Q_2 - \partial_y Q_1) &\sim O(Q_2) + \nu^{-\frac{1}{2}} O(Q_1) \\ &\sim \nu^{\frac{1}{2}} O(S_{11}) + \nu^{-\frac{1}{2}} O(S_{11}) \\ &\sim \nu^{-\frac{1}{2}} O(S_{11}), \end{aligned} \quad (25)$$

which means that the Q_2 contribution to the torque is a factor of ν smaller than the Q_1 contribution in the vorticity equation (12). So it suffices to compute

$$\partial_y Q_1 = \partial_{xy}^2 S_{11} + \partial_{yy}^2 S_{12} \quad (26)$$

in order to calculate ω_s , i.e.

$$\Delta\omega_s = \frac{\partial_y Q_1}{2} + \mathcal{O}(\nu). \quad (27)$$

The equation for Q_1 is constructed by taking the x -derivative of (19) plus the y -derivative of (20)

$$\sin(x) \partial_x Q_1 - Y \cos(x) \partial_Y Q_1 + [1 - \cos(x)] Q_1 - \partial_{YY}^2 Q_1 = -\sin(x) S_{11}, \quad (28)$$

a PDE whose inhomogeneity is a function of S_{11} and whose solution has $Q_1 \sim \mathcal{O}(S_{11})$.

2.3.2. Solution of S_{11}

In order to calculate $\tilde{\mathbf{u}}_s$, we must compute Q_1 , and therefore must explicitly compute S_{11} from (19). Here we show that equation (19) has an exact solution in the form

$$S_{11}(x, Y) = G(x) e^{-\frac{F(x)Y^2}{2}} + H(x) \quad (29)$$

so that

$$\begin{aligned} \partial_Y S_{11} &= -YGF e^{-\frac{FY^2}{2}} \\ \partial_{YY} S_{11} &= -GF [1 - Y^2 F] e^{-\frac{FY^2}{2}} \\ \partial_x S_{11} &= \left[G_x - \frac{Y^2 F_x G}{2} \right] e^{-\frac{FY^2}{2}}. \end{aligned} \quad (30)$$

Substituting (29) into (19) we find three ODEs for F, G, H . The equation for H decouples from the rest and absorbs the homogeneous term

$$\sin(x)H_x + H[1 - 2\cos(x)] - 1 = 0. \quad (31)$$

The equation for F arises by setting the coefficient of $Y^2 e^{-\frac{FY^2}{2}}$ to zero

$$F^2 - \cos(x)F + \frac{\sin(x)F_x}{2} = 0. \quad (32)$$

This is a nonlinear, inhomogeneous, first order equation for $F(x)$. By setting the coefficient of $e^{-\frac{FY^2}{2}}$ to zero we arrive at a first order linear equation for $G(x)$

$$\sin(x)G_x + [1 - 2\cos(x)]G + FG = 0. \quad (33)$$

$H(x)$ will contribute a term to the solution of Q_1 but, since it is independent of x , it will not contribute to the vorticity equation, (26); we do not record its solution. We can see by inspection that the solution to (32) is

$$F(x) = \frac{1 + \cos(x)}{2} = \cos^2\left(\frac{x}{2}\right). \quad (34)$$

Note that the equation (33) is linear, meaning that any multiple of a solution remains a solution. We can write (33) in the form

$$\frac{d(\ln(G))}{dx} = \frac{3(\cos(x) - 1)}{2 \sin(x)} = -\frac{3}{2} \cdot \frac{2 \sin^2\left(\frac{x}{2}\right)}{2 \sin\left(\frac{x}{2}\right) \cos\left(\frac{x}{2}\right)} = -\frac{3}{2} \tan\left(\frac{x}{2}\right) \quad (35)$$

with antiderivative

$$\ln(G(x)) = C + 3 \ln\left(\cos\left(\frac{x}{2}\right)\right) \quad (36)$$

yielding

$$G(x) = S_0 \cos^3\left(\frac{x}{2}\right). \quad (37)$$

So we conclude that the asymptotic form of the primary component of the conformation tensor is

$$S_{11}(x, Y) = S_0 \cos^3\left(\frac{x}{2}\right) e^{-\frac{1}{2} \cos^2\left(\frac{x}{2}\right) Y^2} + H(x). \quad (38)$$

2.3.3. Solution of Q_1

Substituting S_{11} from (38) into equation (28) we now solve

$$\begin{aligned} \sin(x) \partial_x Q_1 - Y \cos(x) \partial_Y Q_1 + [1 - \cos(x)] Q_1 - \partial_{YY}^2 Q_1 = \\ - \sin(x) \left[S_0 \cos^3\left(\frac{x}{2}\right) e^{-\frac{1}{2} \cos^2\left(\frac{x}{2}\right) Y^2} + H(x) \right]. \end{aligned} \quad (39)$$

Again we seek a solution of the form

$$Q_1 = M(x) e^{-\frac{1}{2} \cos^2\left(\frac{x}{2}\right) Y^2} + N(x). \quad (40)$$

It is remarkable that the simple form (40) provides an exact solution of (39), and we provide the details in order to convince the reader. After substituting (40) into (39), we find that the terms which are independent of Y give an equation for $N(x)$

$$\sin(x) \partial_x N + [1 - \cos(x)] N = -\sin(x) H(x) \quad (41)$$

the solution of which requires $H(x)$ from (31). Again, $N(x)$ is not needed since it does not affect the flow.

The partial derivatives of the Gaussian terms are

$$\begin{aligned} \partial_x Q_1 &= \left[M_x + \frac{1}{2} Y^2 M \cos\left(\frac{x}{2}\right) \sin\left(\frac{x}{2}\right) \right] e^{-\frac{1}{2} \cos^2\left(\frac{x}{2}\right) Y^2} \\ \partial_Y Q_1 &= -Y M \cos^2\left(\frac{x}{2}\right) e^{-\frac{1}{2} \cos^2\left(\frac{x}{2}\right) Y^2} \\ \partial_{YY}^2 Q_1 &= M \left[Y^2 \cos^4\left(\frac{x}{2}\right) - \cos^2\left(\frac{x}{2}\right) \right] e^{-\frac{1}{2} \cos^2\left(\frac{x}{2}\right) Y^2}. \end{aligned} \quad (42)$$

Substituting the derivatives from (42) into equation (39) and collecting the coefficients of the Gaussian, we find

$$\begin{aligned} \sin(x) \left[M_x + \frac{1}{2} Y^2 M \cos\left(\frac{x}{2}\right) \sin\left(\frac{x}{2}\right) \right] + \cos(x) Y^2 \cos^2\left(\frac{x}{2}\right) M \\ + [1 - \cos(x)] M + M \cos^2\left(\frac{x}{2}\right) - Y^2 M \cos^4\left(\frac{x}{2}\right) = \\ - \sin(x) S_0 \cos^3\left(\frac{x}{2}\right). \end{aligned} \quad (43)$$

Simplifying with some trigonometric identities, equation (43) becomes

$$\begin{aligned} 2 \sin\left(\frac{x}{2}\right) \cos\left(\frac{x}{2}\right) M_x + Y^2 M \left[\cos\left(\frac{x}{2}\right) \sin\left(\frac{x}{2}\right) \right]^2 + \\ Y^2 M \left[\cos^4\left(\frac{x}{2}\right) - \sin^2\left(\frac{x}{2}\right) \cos^2\left(\frac{x}{2}\right) \right] + 2 \sin^2\left(\frac{x}{2}\right) M + \\ \cos^2\left(\frac{x}{2}\right) M - Y^2 M \cos^4\left(\frac{x}{2}\right) = \\ - 2 S_0 \sin\left(\frac{x}{2}\right) \cos^4\left(\frac{x}{2}\right). \end{aligned} \quad (44)$$

The terms multiplying Y^2 cancel one another, resulting in a linear equation for $M(x)$

$$2 \sin\left(\frac{x}{2}\right) \cos\left(\frac{x}{2}\right) M_x + \left[1 + \sin^2\left(\frac{x}{2}\right) \right] M = -2 S_0 \sin\left(\frac{x}{2}\right) \cos^4\left(\frac{x}{2}\right). \quad (45)$$

whose solution is surprisingly simple,

$$M(x) = -S_0 \sin\left(\frac{x}{2}\right) \cos^2\left(\frac{x}{2}\right). \quad (46)$$

Therefore, the dominant component of the stress divergence is

$$Q_1 = -S_0 \sin\left(\frac{x}{2}\right) \cos^2\left(\frac{x}{2}\right) e^{-\frac{1}{2} \cos^2\left(\frac{x}{2}\right) Y^2} + N(x), \quad (47)$$

where we emphasize that the stretched variable is defined to be $Y = y/\sqrt{\nu}$. The solutions (38) and (47) show that the stress and stress divergence are localized within $\sqrt{\nu}$ of the x -axis. In the far field, they are weighted Dirac δ -distributions.

2.4. Solving for the stress induced velocity, \mathbf{u}_s

Substituting Q_1 from (47) into the vorticity equation (12) and using $\Delta\psi_S = \omega_S$, the induced stream function solves the bi-laplacian equation

$$\Delta^2 \psi_S = \frac{1}{2} \partial_y Q_1 + O(\nu) \quad (48)$$

where

$$\Delta^2 = (\partial_{yy}^2 + \partial_{xx}^2)^2. \quad (49)$$

We will solve this equation in two different ways for the two different regions.

1. In the far field, we approximate the right hand side as the derivative of a δ -distribution and invert the bi-Laplacian on this source.
2. In the near field, we use an anisotropic scaling of the derivatives to simplify the operator on the left hand side. The lowest order terms retain only Y -derivatives.

2.4.1. *The outer approximation*

We define an intermediate variable $\psi_s = \partial_y \phi$ and solve the equation

$$\Delta^2 \phi = -\frac{S_0}{2} \sin\left(\frac{x}{2}\right) \cos^2\left(\frac{x}{2}\right) e^{-\frac{y^2 \cos^2(x/2)}{2\nu}} \quad (50)$$

using the original coordinate y in the far field. The y length scale in the Gaussian is

$$L \sim \frac{\sqrt{2\nu}}{\cos\left(\frac{x}{2}\right)}, \quad (51)$$

which is $O(\sqrt{\nu})$ outside of $||x| - \pi| < \sqrt{\nu}$. Hence for almost all x , with $y > L$, the right hand side of (50) is small. Near $x = \pm\pi$, L is no longer small and the following approximations will fail. However, for (almost all) points outside these turning points, we define the mollified Dirac δ - distribution,

$$\delta_L(y) = \frac{e^{-y^2/L}}{\sqrt{\pi L}}. \quad (52)$$

The smoothed δ -distribution has the property that its integral is 1. Multiplying and dividing by $\sqrt{\pi L}$ we write the ϕ equation as

$$\begin{aligned} \Delta^2 \phi &= -S_0 \sqrt{\frac{\pi \nu}{2}} \sin\left(\frac{x}{2}\right) \cos\left(\frac{x}{2}\right) \delta_L(y) \\ &= -\frac{S_0}{2} \sqrt{\frac{\pi \nu}{2}} \sin(x) \delta_L(y), \end{aligned} \quad (53)$$

and solve for ϕ in the limit $L \rightarrow 0$. Now we can seek a separable solution

$$\phi(x, y) = -\frac{S_0}{2} \sqrt{\frac{\pi \nu}{2}} \sin(x) \Phi(y), \quad (54)$$

where

$$\left(\frac{d^2}{dy^2} - 1\right)^2 \Phi = \delta_0(y). \quad (55)$$

The solution to equation (55) has Φ and its first two partial derivatives continuous at $y = 0$. The jump in the third derivative at $y = 0$ is

$$[\Phi_{yyy}] = 1, \quad (56)$$

which is solved by

$$\Phi = \frac{[1 + |y|]}{4} e^{-|y|}, \quad (57)$$

so that

$$\Phi_y = -\frac{y}{4}e^{-|y|}, \quad (58)$$

and

$$\psi_s = \frac{S_0}{8} \sqrt{\frac{\pi \nu}{2}} \sin(x) y e^{-|y|}. \quad (59)$$

Therefore, the induced velocity field is

$$\begin{bmatrix} u_s \\ v_s \end{bmatrix} = -\frac{S_0}{8} \sqrt{\frac{\pi \nu}{2}} \begin{bmatrix} \sin(x) (1 - |y|) \\ -y \cos(x) \end{bmatrix} e^{-|y|}. \quad (60)$$

The original hypothesis was that the induced velocity field, \mathbf{u}_s should have the same functional form as the total velocity field, $\tilde{\mathbf{u}}$ near where the stress is maximum. Clearly (60) and (14) do not have the same form everywhere. However, the stress is sharply localized in a layer of width $L \sim \sqrt{\nu} \ll 1$ near $y = 0$, where the induced velocity is approximately

$$\begin{bmatrix} u_s \\ v_s \end{bmatrix} \approx -\frac{S_0}{8} \sqrt{\frac{\pi \nu}{2}} \begin{bmatrix} \sin(x) \\ -y \cos(x) \end{bmatrix} + \dots \quad (61)$$

which is proportional to $\tilde{\mathbf{u}}$ from (14).

2.4.2. The inner approximation

In order to get the correct solution of the velocity near and within the stress island, we must consider this boundary layer region again using the scaled y variable. Upon substituting equation (47) into (48), using the definition of Y , retaining the largest terms on the left hand side, and integrating once with respect to y , we find

$$\frac{1}{\nu^{3/2}} \partial_{YY}^3 \psi_s = -\frac{S_0}{2} \sin\left(\frac{x}{2}\right) \cos^2\left(\frac{x}{2}\right) e^{-\frac{1}{2} \cos^2\left(\frac{x}{2}\right) Y^2}. \quad (62)$$

Defining a scaled boundary layer variable

$$z = \frac{\cos\left(\frac{x}{2}\right)}{\sqrt{2}} Y, \quad (63)$$

and the stream function equation becomes

$$\frac{d^3}{dz^3} \psi_s = -S_0 \sqrt{2\nu^3} \tan\left(\frac{x}{2}\right) e^{-z^2}. \quad (64)$$

After integrating three times, we arrive at the solution

$$\psi_s = -S_0 \sqrt{2\nu^3} \tan\left(\frac{x}{2}\right) \left\{ \frac{\sqrt{\pi}}{8} [2z^2 + 1] \operatorname{erf}(z) + \frac{z}{4} e^{-z^2} + c_1 z \right\}, \quad (65)$$

where c_1 is constant with respect to Y , although not necessarily with respect to x . In order to match the y -dependence of ψ_s , we evaluate ψ_s from the outer

solution in equation (59) in the limit $y \rightarrow 0$, compare it to ψ_s in the inner solution, and substitute the definition $z = \frac{\cos(\frac{x}{2})y}{\sqrt{2\nu}}$.

The large z limit of the near field solution is

$$\begin{aligned}
\lim_{z \rightarrow \infty} \psi_s &= -S_0 \sqrt{2\nu^3} \tan\left(\frac{x}{2}\right) \left\{ \frac{\sqrt{\pi}}{4} z^2 + c_1 z \right\} \\
&= -S_0 \sqrt{2\nu^3} \tan\left(\frac{x}{2}\right) \left\{ \frac{\sqrt{\pi}}{4} \frac{\cos^2\left(\frac{x}{2}\right)}{2\nu} y |y| + c_1 \frac{\cos\left(\frac{x}{2}\right)}{\sqrt{2\nu}} y \right\} \\
&= -S_0 \sqrt{2\nu^3} \sin\left(\frac{x}{2}\right) \left\{ \frac{\sqrt{\pi}}{4} \frac{\cos\left(\frac{x}{2}\right)}{2\nu} y |y| + \frac{c_1 y}{\sqrt{2\nu}} \right\}.
\end{aligned} \tag{66}$$

The term which is quadratic in y matches the outer solution automatically. The linear term in y matches the outer solution if

$$c_1 = -\frac{\cos\left(\frac{x}{2}\right)}{4} \sqrt{\frac{\pi}{2\nu}}. \tag{67}$$

Near $y = 0$, the near field approximation yields the horizontal velocity

$$\begin{aligned}
u_s &= -\partial_y \psi_s \\
&= -\frac{\cos\left(\frac{x}{2}\right)}{\sqrt{2\nu}} \partial_z \psi_s \\
&\approx S_0 \nu \sin\left(\frac{x}{2}\right) \left\{ \frac{1}{4} + \frac{1}{4} + c_1 \right\} \\
&\approx S_0 \nu \sin\left(\frac{x}{2}\right) \left\{ \frac{1}{2} - \frac{\cos\left(\frac{x}{2}\right)}{4} \sqrt{\frac{\pi}{2\nu}} \right\} \\
&\approx -\frac{S_0}{8} \sqrt{\frac{\pi\nu}{2}} \left[\sin(x) - 4\sqrt{\frac{2\nu}{\pi}} \sin\left(\frac{x}{2}\right) \right].
\end{aligned} \tag{68}$$

Notice a few features of the near field horizontal velocity. First, we have only retained terms independent of y because we only need to study u_s on the axis. Next, the first term matches the first term in the far field approximation and is the leading order term in the near field, while the second term is $\mathcal{O}(\sqrt{\nu})$ smaller. The second term describes a shrinking of the horizontal extent of the horizontal velocity by $\mathcal{O}(\sqrt{\nu})$, i.e. the zonal velocity is zero on $y = 0$ at x_* where

$$\cos\left(\frac{x_*}{2}\right) = \sqrt{\frac{8\nu}{\pi}} \implies x_* \approx \pi - 4\sqrt{\frac{2\nu}{\pi}}. \tag{69}$$

This further implies that a line of stress islands along $y = 0$ will be drawn to one another by their tendency to pull their endpoints toward their centers.

2.4.3. Stress islands on a periodic domain

The stream function in (59) accounts for stress islands on an x -periodic, but not y -periodic, domain. In order to account for y -periodicity, we need to solve (55) with a periodized δ function. Solutions to the periodic version of (55) on $0 < y < 2\pi$ are exponentials and y times exponentials, which can be written

$$\Phi = A \cosh(y - \pi) + B(y - \pi) \sinh(y - \pi) + C \sinh(y - \pi) + D(y - \pi) \cosh(y - \pi). \quad (70)$$

The function is centered at $y = \pi$ in order to exploit the symmetry around this point. In fact, Φ should be symmetric around this point (two derivatives of Φ are proportional to u) so we can simplify the expression

$$\Phi = A \cosh(y - \pi) + B(y - \pi) \sinh(y - \pi). \quad (71)$$

Establishing periodicity in the y -direction requires

$$\begin{aligned} \Phi(2\pi) &= \Phi(0), & \Phi_{yy}(2\pi) &= \Phi_{yy}(0), \\ \Phi_y(2\pi) &= \Phi_y(0), & \Phi_{yyy}(2\pi) &= \Phi_{yyy}(0) - 1. \end{aligned} \quad (72)$$

The choice of symmetric Φ means that its second derivative automatically satisfies the periodicity conditions, and one need only use the first and third derivative conditions. The first derivative is

$$\Phi_y = (A + B) \sinh(y - \pi) + B(y - \pi) \cosh(y - \pi), \quad (73)$$

which, when enforcing periodicity results in

$$A = -B(1 + \pi \coth(\pi)), \quad (74)$$

so that

$$\begin{aligned} \Phi &= B [(y - \pi) \sinh(y - \pi) - (1 + \pi \coth(\pi)) \cosh(y - \pi)] \\ \Phi_y &= B [(y - \pi) \cosh(y - \pi) - \pi \coth(\pi) \sinh(y - \pi)] \\ \Phi_{yy} &= B [(1 - \pi \coth(\pi)) \cosh(y - \pi) + (y - \pi) \sinh(y - \pi)] \\ \Phi_{yyy} &= B [(2 - \pi \coth(\pi)) \sinh(y - \pi) + (y - \pi) \cosh(y - \pi)]. \end{aligned} \quad (75)$$

Lastly, using the third derivative condition yields

$$B = \frac{-1}{4 \sinh(\pi)}. \quad (76)$$

Using Φ_y to construct ψ_P (P is used to denote ‘‘periodic’’) we find

$$\psi_P = \frac{S_0 \coth(\pi)}{8} \sqrt{\frac{\pi\nu}{2}} \sin(x) \left[(y - \pi) \frac{\cosh(y - \pi)}{\cosh(\pi)} - \pi \frac{\sinh(y - \pi)}{\sinh(\pi)} \right], \quad (77)$$

on $0 < y < 2\pi$. It must be periodically extended outside of this domain, for example to $-2\pi < y < 0$,

$$\psi_P = \frac{S_0 \coth(\pi)}{8} \sqrt{\frac{\pi\nu}{2}} \sin(x) \left[(y + \pi) \frac{\cosh(y + \pi)}{\cosh(\pi)} - \pi \frac{\sinh(y + \pi)}{\sinh(\pi)} \right]. \quad (78)$$

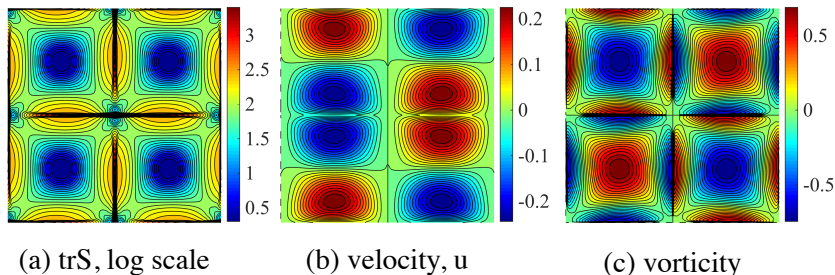


Figure 1: 4-roll mill simulations on $[0, 2\pi]^2$ with $\nu = 0.00025$, $Wi = 20$

2.4.4. Multiple stress islands on a doubly periodic domain

In [27, 18], a doubly periodic 4-roll mill type geometry was studied on $[0, 2\pi] \times [0, 2\pi]$. The background force $\mathbf{f} = (2 \sin x \cos y, -2 \cos x \sin y)$ prescribed a flow with an extensional point at the origin, stretching in the x -direction and squeezing in the y -direction. The results of numerical simulations of this flow for $Wi = 20$, $\nu = 0.00025$ are plotted in in Fig. 1 after a time $t = 5Wi$ when the flow has equilibrated. Fig.1 (a) shows contours of the trace of the conformation tensor $S_{11} + S_{22}$, on a log-scale, (b) shows the first component of the velocity u , and (c) the vorticity $\partial_x v - \partial_y u$. Unlike our theoretical background flow, here there are four stress islands contributing to the flow in the domain $0 < x < \pi, 0 < y < \pi$. In order to compare our theoretical predictions with this flow geometry we need to account for all of these stress islands, we will show results of the comparison in Sec. 3

For the island oriented parallel to the x -axis located at $(x_1, y_1) = (\pi, \pi)$, we need to use the expression in (78), but shift its location,

$$\begin{aligned}
 \psi_1 &= \frac{S_0 \coth(\pi)}{8} \sqrt{\frac{\pi\nu}{2}} \sin(x - x_1) \\
 &\quad \left[(y - y_1 + \pi) \frac{\cosh(y - y_1 + \pi)}{\cosh(\pi)} - \pi \frac{\sinh(y - y_1 + \pi)}{\sinh(\pi)} \right] \\
 &= -\frac{S_0 \coth(\pi)}{8} \sqrt{\frac{\pi\nu}{2}} \sin(x) \left[y \frac{\cosh(y)}{\cosh(\pi)} - \pi \frac{\sinh(y)}{\sinh(\pi)} \right].
 \end{aligned} \tag{79}$$

The other two islands are rotated by $\pi/2$, which is effected by the replacement $(x, y) \rightarrow (y, -x)$. The island along the y -axis is located at $(x_2, y_2) = (0, \pi)$ and from its perspective, the first quadrant is “below” it, so we again use the

expression in (78). Therefore

$$\begin{aligned}\psi_2 &= \frac{S_0 \coth(\pi)}{8} \sqrt{\frac{\pi\nu}{2}} \sin(y - y_2) \\ &\quad \left[(-x - x_2) + \pi \frac{\cosh(-x - x_2) + \pi}{\cosh(\pi)} - \pi \frac{\sinh(-x - x_2) + \pi}{\sinh(\pi)} \right] \quad (80) \\ &= \frac{S_0 \coth(\pi)}{8} \sqrt{\frac{\pi\nu}{2}} \sin(y) \left[(x - \pi) \frac{\cosh(x - \pi)}{\cosh(\pi)} - \pi \frac{\sinh(x - \pi)}{\sinh(\pi)} \right].\end{aligned}$$

Finally we consider the island at $(x_3, y_3) = (\pi, 0)$; from the perspective of this stresslet the first quadrant is “above” it, meaning that the expression in (77) is relevant,

$$\begin{aligned}\psi_3 &= \frac{S_0 \coth(\pi)}{8} \sqrt{\frac{\pi\nu}{2}} \sin(y - y_3) \\ &\quad \left[-(x - x_3) - \pi \frac{\cosh(-x - x_3) - \pi}{\cosh(\pi)} - \pi \frac{\sinh(-x - x_3) - \pi}{\sinh(\pi)} \right] \quad (81) \\ &= -\frac{S_0 \coth(\pi)}{8} \sqrt{\frac{\pi\nu}{2}} \sin(y) \left[x \frac{\cosh(x)}{\cosh(\pi)} - \pi \frac{\sinh(x)}{\sinh(\pi)} \right].\end{aligned}$$

Notice that each of the ψ expressions is positive in $(x, y) \in [0, \pi] \times [0, \pi]$, which means that they are additive, i.e., the induced flow from each of the four stress islands reinforce the flow from the others. Notice also that ψ_1 and ψ_2 are the same expression with x and y interchanged, as are ψ_1 and ψ_3 .

The sum of the four expressions yields

$$\psi_{tot} = \frac{S_0 \coth(\pi)}{8} \sqrt{\frac{\pi\nu}{2}} [\sin(x)M(y) + \sin(y)M(x)], \quad (82)$$

where the function

$$M(x) \equiv \left[\frac{(x - \pi) \cosh(x - \pi) - x \cosh(x)}{\cosh(\pi)} - \pi \frac{\sinh(x - \pi) - \sinh(x)}{\sinh(\pi)} \right]. \quad (83)$$

2.5. Calculating S_0

Near $y = 0$, we expect the **total** velocity,

$$\begin{bmatrix} u \\ v \end{bmatrix} = \begin{bmatrix} \sin(x) \\ -y \cos(x) \end{bmatrix} \quad (84)$$

to consist of an externally forced portion

$$\begin{bmatrix} u_f \\ v_f \end{bmatrix} = Wi \begin{bmatrix} \sin(x) \\ -y \cos(x) \end{bmatrix}, \quad (85)$$

and a stress induced portion

$$\begin{bmatrix} u_S \\ v_S \end{bmatrix} = (1 - Wi) \begin{bmatrix} \sin(x) \\ -y \cos(x) \end{bmatrix}. \quad (86)$$

We need to compare this form of the velocity field with the solution in equation (82) evaluated near the origin. The function $M(x)$ in equation (83) can be approximated as $1.144 \sin(x)$, near $x = 0$, so near the origin

$$\psi_{tot} \approx \frac{S_0 \alpha}{8} \sqrt{\frac{\pi \nu}{2}} \sin(x) \sin(y), \quad (87)$$

where $\alpha = 2 \coth(\pi) M'(0) \approx 2 \coth(\pi) \times 1.144 \approx 2.297$. Comparing (87) with (86) we find

$$\frac{S_0}{8} \sqrt{\frac{\pi \nu}{2}} \alpha = Wi - 1 \quad \text{or} \quad S_0 = \frac{8(Wi - 1)}{\alpha} \sqrt{\frac{2}{\pi \nu}}. \quad (88)$$

In Section 3 we will compare this theoretical prediction to simulations of the Stokes-Oldroyd-B system. In the case of the singly periodic velocity field $\alpha = 1$, however we do not have any numerical simulations with which to compare this result.

2.6. The correctly scaled velocity field.

The original rescaling of the velocity field by the Weissenberg number was simply a computational convenience. We must remove this scaling in order to get the actual velocity field

$$\mathbf{u} = \frac{\tilde{\mathbf{u}}}{Wi}. \quad (89)$$

In the case of the singly periodic velocity field, the background velocity,

$$\begin{bmatrix} u_f \\ v_f \end{bmatrix} = \begin{bmatrix} \sin(x) \\ -y \cos(x) \end{bmatrix} \quad (90)$$

is independent of the Weissenberg number, as it must be from equation (4). The stress induced velocity field is

$$\begin{bmatrix} u_s \\ v_s \end{bmatrix} = \left(\frac{1}{Wi} - 1 \right) \begin{bmatrix} \sin(x) (1 - |y|) \\ -y \cos(x) \end{bmatrix} e^{-|y|}, \quad (91)$$

so that the total stream function is

$$\psi = -y \sin(x) \left[1 + \left(\frac{1}{Wi} - 1 \right) e^{-|y|} \right]. \quad (92)$$

Near the stress island, the velocity scales as the reciprocal of Wi , but far away the stress induced response decays. The same rescaling yields the stream function for the doubly periodic example,

$$\psi = -\sin(x) \sin(y) + \left(1 - \frac{1}{Wi} \right) \left[\frac{\sin(x)M(y) + \sin(y)M(x)}{2M'(0)} \right]. \quad (93)$$

3. Comparison to Numerical Simulations

We compare our theoretical results to numerical simulations of the Stokes-Oldroyd-B system defined in Eqs.(4)-(5) where \mathbf{f} creates a doubly periodic 4-roll mill type geometry,

$$\mathbf{f} = (2 \sin x \cos y, -2 \cos x \sin y). \quad (94)$$

The system is solved in a doubly periodic domain using a pseudo-spectral method ([27, 18]). These simulations were performed with $\Delta x = 2\pi/N$, for $N = 2^9$, with $\nu = 0.0125, 0.0025, 0.00125, 0.00025$, where $\nu/(\Delta x)^2 \approx 83, 17, 8, 2$.

| ν | $Wi = 10$ | $Wi = 15$ | $Wi = 20$ |
|---------|-----------|-----------|-----------|
| 0.01250 | 0.08250 | 0.04338 | 0.00613 |
| 0.00250 | 0.02542 | 0.01073 | 0.0035 |
| 0.00125 | 0.00785 | 0.01107 | 0.00575 |
| 0.00025 | 0.04153 | 0.00694 | 0.00322 |

Table 1: Relative difference in theoretical maximum, $S_{11}(0,0)$, compared with 4-roll mill simulation.

In Table (1) we show the relative difference between the theoretical prediction in Eq. (88) and the maximum of the first component of the stress tensor at equilibration for the 4-roll mill simulations, using the value $\alpha = 2.297 \approx 2 \coth(\pi) \times 1.144$, in our calculation of S_0 from equation (88). The error in the approximation is smallest for $Wi = 10, 20$ for $\nu = 0.00125$, and for $Wi = 15$ is smallest for $\nu = 0.00025$, where the error $\lesssim 1\%$. We see that we can get excellent matching between the theoretical prediction and the numerical solutions when the diffusion is approximately 2 – 8 times $(\Delta x)^2$.

Decreasing the diffusion without increasing resolution will increase the error in the numerical simulation since we need a grid size $\Delta x < \sqrt{\nu}/C$, for some number $C > 2$, which is independent of ν . On the other hand, increasing ν increases the error in the asymptotic approximation. Therefore the asymptotic approximation becomes more valid at small values of the stress diffusion - which is precisely where high resolution is needed in numerical methods, thereby greatly increasing computational time.

In our asymptotic solution, the maximum of the conformation tensor scales with $\frac{1}{\sqrt{\nu}}$. While we do not expect $S_{11}(0,0)$ to converge as $\nu \rightarrow 0$ we do, however, expect the conformation tensor to converge in an integral-norm; it is precisely this integral quantity that is necessary to find the solution for the velocity. Simulations in the 4-roll geometry show that the integral is converging. In Fig. 2 we plot the relative error in the L^1 -norm of the trace of the conformation tensor, defined by

$$L^1(\text{tr}\mathbf{S}) \equiv \int_0^{2\pi} \int_0^{2\pi} |\text{tr}\mathbf{S}| \, dx \, dy,$$

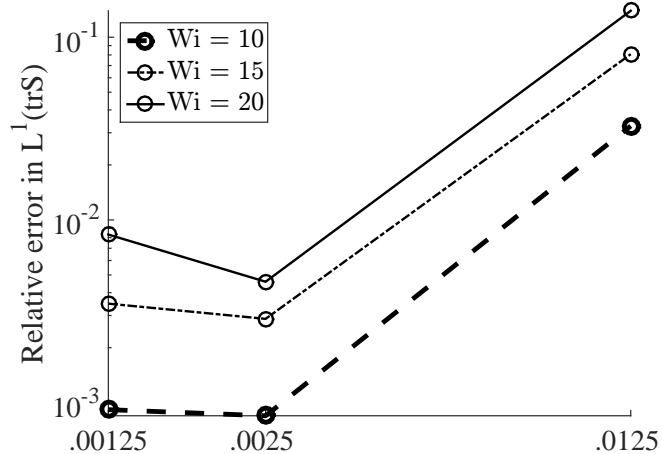


Figure 2: Relative error in $L^1(\text{tr}\mathbf{S})$ as a function of ν , comparing with solution at $\nu = 0.00025$.

where we use the solution with diffusion coefficient $\nu = 0.00025$ as the “true” solution. The maximum of the conformation tensor may be growing as $\nu \rightarrow 0$, but the integral of this quantity converges as $\nu \rightarrow 0$, and in fact for the values considered, the relative size is changing by less than one percent.

It is not just at the extensional stagnation point where we see good agreement between theory and simulation. In a strip around the y -axis (and by symmetry along all the directions of stretching and compression in the 4-roll mill) the asymptotic theory captures the lowest order behavior of the velocity. For example we compare the theoretically predicted horizontal velocity along

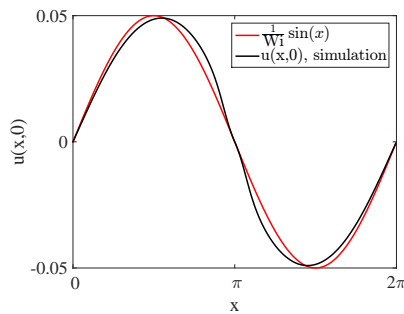


Figure 3: Comparison of simulation $u(x,0)$ with theoretically predicted $\frac{1}{Wi} \sin(x)$, simulations use $Wi = 20$, $\nu = 0.00025$

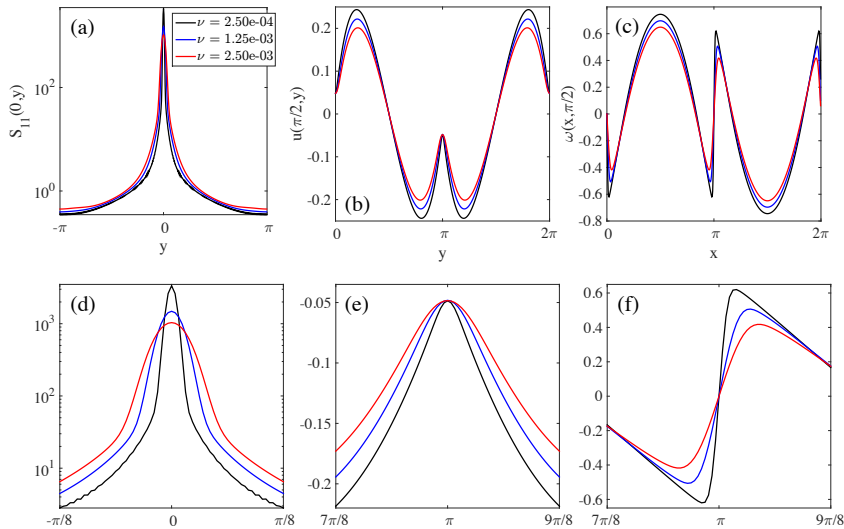


Figure 4: 4-roll mill simulations for $Wi = 20$, for $\nu = 0.0025, 0.00125, 0.00025$ (a) principal component of conformation tensor along axis of compression $S_{11}(0, y)$ (b) velocity $u(\pi/2, y)$ (c) vorticity $\omega(x, \pi/2)$ (d)-(f) close-ups of (a)-(c) respectively

$y = 0$ with the simulation. From equations 90–91, the former is given by

$$u(x, y)|_{y=0} = \sin(x) + \left(\frac{1}{Wi} - 1 \right) \sin(x) (1 - |y|) e^{-|y|} = \frac{1}{Wi} \sin(x).$$

Figure 3 shows plots of both $\frac{1}{Wi} \sin(x)$ and simulation results of $u(x, 0)$ for

| ν | $Wi = 10$ | $Wi = 15$ | $Wi = 20$ |
|---------|-----------|-----------|-----------|
| 0.01250 | 0.03878 | 0.03397 | 0.02847 |
| 0.00250 | 0.04802 | 0.04374 | 0.03299 |
| 0.00125 | 0.04814 | 0.04483 | 0.03823 |
| 0.00025 | 0.04577 | 0.03675 | 0.02927 |

Table 2: Relative difference between theoretical and simulation in $u(\pi/2, 0)$ compared with 4-roll mill simulation.

$Wi = 20$, $\nu = 0.00025$. Results of relative error in the approximation at $x = \pi/2$ for a range of Wi , and ν are given in Table 2. This approximation is valid for all ν in the asymptotically small limit since this solution does not depend on diffusion. The error remains small in a strip around the axes of compression and extension near the stagnation point for $|y| \lesssim 0.1$.

Now let us examine the dependence of the numerical solution on the stress diffusion, ν , in the 4-roll mill numerical simulations. Figure 4 (a) shows the first component of the conformation tensor along the y -axis, in the direction of compression and Fig. 4 (d) is a close-up of (a). The Gaussian structure is evident, and looking at the close-up of the conformation tensor (d) we see a

sharp second derivative near the origin located where the solution transitions from the singular behavior of the Gaussian, to the smoother behavior at the center of the 4-roll mill (where the flow extension is weak).

Figure 4 (b) and close-up (e) show the horizontal velocity in a vertical cut through the center of the 4-roll mill, $x = \pi/2$. Near $y = \pi$ the stress tensor is again singular. The dip in the horizontal velocity is distinctly evident in both figures. As described above, this dip is due to the response of the horizontal velocity to the stress island. The strength of the velocity at the center of the stress island, $(x, y) = (\pi/2, \pi)$ is not sensitive to ν and clearly attains the value $u = Wi^{-1} = .05$ at the center of the dip, as is predicted in the asymptotic theory.

Finally, Fig. 4 (c) and close-up (f), show that the vorticity has a jump which is smoothed out by diffusion, but the magnitude of the jump converges with decreasing diffusion and in the limit of $\nu = 0$, the asymptotic model predicts

$$\lim_{x \rightarrow \pi^-} \omega(x, \pi/2) = (1 - Wi^{-1}) \frac{M''(0)}{2M'(0)} \approx -0.775. \quad (95)$$

Extrapolating the numerically computed ω linearly to $x = \pi^-$ yields $\omega \approx -0.725$, in excellent agreement with the asymptotic prediction.

Matching the stress island to the center of the roll is a more difficult problem, and since the 4-roll mill is a toy geometry, performing the detailed calculations necessary to do the matching is unlikely to yield further insight. However, near the center of the roll, the flow is purely rotational and is dominated by the antisymmetric part of the velocity gradient matrix. Therefore, irrespective of the Weissenberg number, the flow near the center of the 4-roll mill behaves like the low Wi limit because the symmetric part of the deformation tensor, which stretches the flow and creates the stress islands, is small.

We posit that the stress tensor can be written $\mathbf{S} = \mathbf{S}_R + \mathbf{S}_S$ where \mathbf{S}_R denotes the regular solution, which dominates in the middle of the rolls, and \mathbf{S}_S denotes the singular solution which describes the stress islands (and which we have already discussed in detail). Using the intuition that the flow at the center of the roll behaves like the low Wi flow locally, then $\mathbf{S}_R \approx \mathbb{I} + Wi(\nabla \mathbf{u} + \nabla \mathbf{u}^T)$ [27]. Taking the curl of Eq. (4), and substituting $\mathbf{S} = \mathbf{S}_R + \mathbf{S}_S$ gives

$$\Delta \omega = -\frac{\Delta \omega}{2} - 4 \sin(x) \sin(y). \quad (96)$$

This gives a value for $\Delta \omega$ at the center of the 4-roll mill,

$$-\Delta \omega = \frac{8}{3} \implies -\frac{\Delta \omega}{2} = \frac{4}{3}. \quad (97)$$

For all $\nu = 0.0125, 0.025, 0.00125, 0.00025$ and $Wi = 10, 15, 20$ the error in this value at the center of the roll is less than 0.04%. Although this solution is obtained in the low Wi limit, it is valid for all Wi . Note that near the axes of extension and compression this regular solution only has terms that are lower order in our expansion and can be ignored.

Finally, we make a comment about using diffusion to enforce finite-extension. In the UCM model of viscoelastic fluids, an asymptotic scaling argument was used to show that at extensional points the width of a birefringent strand in the FENE-P model scales as $\frac{1}{\ell} + \frac{1-\ln \ell}{2\ell} \frac{1}{Wi} + \mathcal{O}(\frac{1}{Wi^2})$ [28]. As the Gaussian full width at half-maximum given in S_0 scales like $\sqrt{\nu}$ which in turn scales like $\frac{1}{\ell^2}$, we see that the birefringent strand constructed using diffusion will be much thinner than a corresponding strand using FENE-P. The FENE-P model still requires some diffusion to evolve to steady state, in order to resolve the corners that arise in the cut-off of $\text{tr } \mathbf{S}$ that arises at extensional stagnation points in FENE-P [27]. It may be possible to use far less diffusion to regularize FENE-P and obtain accurate solutions. An argument like we made above would be more complicated in that case, but if possible, it would be an important result.

4. Conclusions

We have found an analytic, asymptotic approximation of the steady-state equations for viscoelastic creeping flow in a neighborhood of an extensional stagnation point. This approximation uses polymer stress diffusion as a regularization to find a solution in the form of a Gaussian for the principle component of the polymer stress in the stretching direction.

At the extensional point, the stress becomes localized and highly stretched in a region of the outgoing streamlines of the stagnation point. The Gaussian structure of the solution was recognized in [18], but without including the x -dependence in the solution it is not possible to get any information about the feedback to the velocity. This paper used the special structure of the equations that arises when $u_y = 0$, which allows solutions to be obtained in orders of the asymptotic parameter, ν . The singular solutions capture the behavior of the elastic stress near the stagnation point, and can be used to find an approximation for the velocity response near the stagnation point.

Due to the special structure of the equations this solution for the velocity is *independent* of the diffusion parameter. This shows that the exact nature of the elastic stress at the extensional point is *not essential* to determine the behavior of the flow near the stagnation point. This is an important observation since many of the modifications to Oldroyd-B that are designed to incorporate finite extension or other rheological properties, such as FENE-P, Giesekus, PTT, inherit the difficulties of Oldroyd-B near extensional points. This indicates that a small amount of diffusion, chosen carefully to depend on both the parameters of the flow and on how the flow turns around, can be used to determine an appropriate grid-size and diffusion for the problem that will exhibit sufficient smoothness as well as the ability to stretch to a physically valid length.

This solution also gives an essential theoretical piece of the physical explanation for the instabilities in viscoelastic fluids that may lead to a deeper understanding of elastic turbulence. We have shown that the velocity response to large stress is to decrease the vorticity near the regions of large stress which in turn leaves room for stress to grow. Thus stress expels vorticity, which in turn creates stress.

J.A.B. was partially supported by NSF DMS 1009959 and 1313477.

References

- [1] P. E. Arratia, C. Thomas, J. Diorio, J. Gollub, Elastic instabilities of polymer solutions in cross-channel flow, *Physical review letters* 96 (14) (2006) 144502.
- [2] J. Soulages, M. Oliveira, P. Sousa, M. Alves, G. McKinley, Investigating the stability of viscoelastic stagnation flows in t-shaped microchannels, *Journal of Non-Newtonian Fluid Mechanics* 163 (1) (2009) 9–24.
- [3] B. Liu, M. Shelley, J. Zhang, Oscillations of a layer of viscoelastic fluid under steady forcing, *Journal of Non-Newtonian Fluid Mechanics* 175 (2012) 38–43.
- [4] S. Haward, G. McKinley, Instabilities in stagnation point flows of polymer solutions, *Physics of Fluids (1994-present)* 25 (8) (2013) 083104.
- [5] P. Sousa, F. Pinho, M. Oliveira, M. Alves, Purely elastic flow instabilities in microscale cross-slot devices, *Soft matter* 11 (45) (2015) 8856–8862.
- [6] O. Harris, J. Rallison, Start-up of a strongly extensional flow of a dilute polymer solution, *Journal of non-newtonian fluid mechanics* 50 (1) (1993) 89–124.
- [7] O. Harris, J. Rallison, Instabilities of a stagnation point flow of a dilute polymer solution, *Journal of non-newtonian fluid mechanics* 55 (1) (1994) 59–90.
- [8] R. Poole, M. Alves, P. Oliveira, Purely elastic flow asymmetries, *Physical review letters* 99 (16) (2007) 164503.
- [9] B. Thomases, M. Shelley, Transition to mixing and oscillations in a stokesian viscoelastic flow, *Physical review letters* 103 (9) (2009) 094501.
- [10] L. Xi, M. D. Graham, A mechanism for oscillatory instability in viscoelastic cross-slot flow, *Journal of Fluid Mechanics* 622 (2009) 145–165.
- [11] B. Thomases, M. Shelley, J.-L. Thiffeault, A stokesian viscoelastic flow: Transition to oscillations and mixing, *Physica D: Nonlinear Phenomena* 240 (20) (2011) 1602–1614.
- [12] H. Giesekus, Die elastizität von flüssigkeiten, *Rheologica Acta* 5 (1) (1966) 29–35.
- [13] N. P. Thien, R. I. Tanner, A new constitutive equation derived from network theory, *Journal of Non-Newtonian Fluid Mechanics* 2 (4) (1977) 353–365.

- [14] A. Peterlin, Streaming birefringence of soft linear macromolecules with finite chain length, *Polymer* 2 (1961) 257–264.
- [15] R. B. Bird, O. Hassager, R. Armstrong, C. Curtiss, *Dynamics of Polymeric Liquids*, Vol. 2: Kinetic Theory, John Wiley and Sons, 1980.
- [16] R. G. Owens, T. N. Phillips, *Computational rheology*, Vol. 2, World Scientific, 2002.
- [17] R. D. Guy, B. Thomases, Computational challenges for simulating strongly elastic flows in biology, in: *Complex Fluids in Biological Systems*, Springer, 2014, pp. 361–400.
- [18] B. Thomases, An analysis of the effect of stress diffusion on the dynamics of creeping viscoelastic flow, *J. Non-Newton. Fluid Mech* 166 (2011) 1221–1228.
- [19] P. Constantin, M. Kliegl, Note on global regularity for two-dimensional oldroyd-b fluids with diffusive stress, *Archive for Rational Mechanics and Analysis* (2012) 1–16.
- [20] R. G. Larson, *The structure and rheology of complex fluids*, Vol. 2, Oxford university press New York, 1999.
- [21] A. W. El-Kareh, L. G. Leal, Existence of solutions for all Deborah numbers for a non-Newtonian model modified to include diffusion, *J. Non-Newton. Fluid Mech.* 33 (1989) 257.
- [22] R. Sureshkumar, A. N. Beris, Effect of artificial stress diffusivity on the stability of numerical calculations and the flow dynamics of time-dependent viscoelastic flows, *Journal of Non-Newtonian Fluid Mechanics* 60 (1995) 53 – 80.
- [23] A. Lyazid, O. Scrivener, R. Teitgen, Velocity field in an elongational polymer solution flow, in: *Rheology*, Springer, 1980, pp. 141–148.
- [24] K. Gardner, E. Pike, M. Miles, A. Keller, K. Tanaka, Photon-correlation velocimetry of polystyrene solutions in extensional flow fields, *Polymer* 23 (10) (1982) 1435–1442.
- [25] Y. Rabin, F. S. Henyey, D. B. Creamer, Flow modification by polymers in strong elongational flows, *The Journal of chemical physics* 85 (8) (1986) 4696–4701.
- [26] O. Harlen, J. Rallison, M. Chilcott, High-deborah-number flows of dilute polymer solutions, *Journal of Non-Newtonian Fluid Mechanics* 34 (3) (1990) 319–349.
- [27] B. Thomases, M. Shelley, Emergence of singular structures in Oldroyd-B fluids, *Phys. Fluids* 19 (2007) 103103.

- [28] P. Becherer, A. N. Morozov, W. v. Saarloos, Scaling of singular structures in extensional flow of dilute polymer solutions, *Journal of Non-Newtonian Fluid Mechanics* 153 (2) (2008) 183–190.